ARTICLE

Negatively Charged Ions to Probe Self-Assembled Monolayers Reorganization Driven by Interchain Interactions

Received 00th January 20xx,
Accepted 00th January 20xx

DOI: 10.1039/x0xx00000x

Angelo Tricase[a], Angela Stefanachi[b], Rosaria Anna Picca[a], Eleonora Macchia[c], Alessandro Favia[d,e], Francesco Leonetti[b], Gaetano Scamarcio[e,f], Davide Blasi[a,d,*], Paolo Bollella[a,*], and Luisa Torsi [a, c ,d]

A combined cyclic voltammetry (CV) and grazing angle – attenuated total reflectance (GA-ATR) IR study on the interchain interaction driven reorganization of self-assembled monolayers (SAMs) in an electric field, is presented. The study focuses on an N-(2-hydroxyethyl)-3-mercaptopropanamide (NMPA) SAM endowed with interchain hydrogen bondings, strongly affected by an external electric field interacting with dipole moment associated to the hydrogen bonding. Conversely, a 1-hexanethiol SAM is characterized by interchain hydrophobic interaction not affected by the applied field. These features have been demonstrated by means of reiterated CV experiments involving an electroactive negatively charged probe, namely $Fe(CN)_6^{4-}$ and the Au-SAM serving as working electrode. The diffusional/interpenetration kinetics parameters return the apparent electron transfer rate constant (k_0) values. For the NMPA, the interchain rearrangement kinetics was that of an ion-permeable layer that reached, in the electric field, a steady-state configuration after about 50 minutes. The 1-hexanethiol chains' reorganization exhibited a more complex kinetic involving a first phase (*ca.* 50 minutes) of a ion-permeable phase followed by a sharp decrease in the anodic peak current related to the tightening of structure, likely due to interchain hydrophobic interaction, hindering ions diffusion. The change in the SAM structure upon cycling in the electric field was confirmed by the GA-ATR measurements.

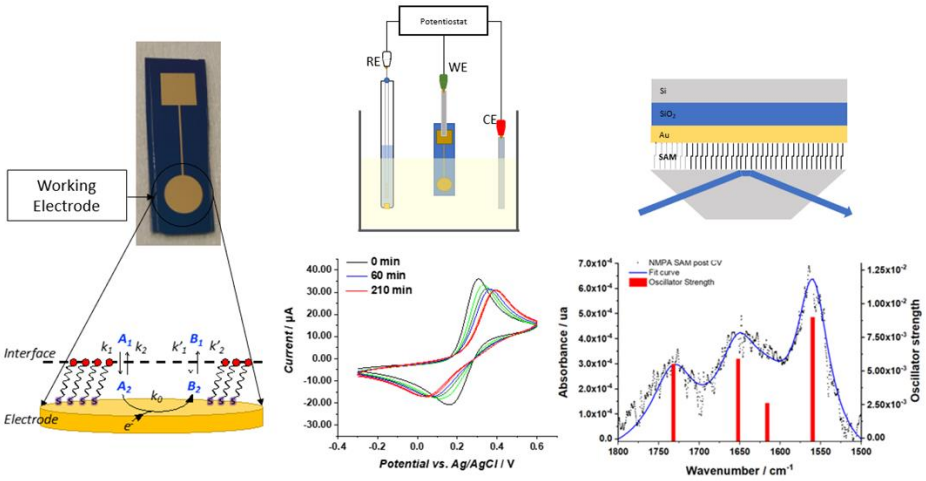

[a.] *Dipartimento di Chimica, Università degli Studi di Bari Aldo Moro, 70125 Bari (Italy).*
[b.] *Dipartimento di Farmacia – Scienze del Farmaco, Università degli Studi di Bari Aldo Moro, 70125 Bari, Italy*
[c.] *The Faculty of Science and Engineering, Åbo Akademi University, 20500 Turku (Finland)*
[d.] *CSGI (Centre for Colloid and Surface Science), 70125 Bari (Italy)*
[e.] *Dipartimento Interateneo di Fisica "M. Merlin", Università degli Studi di Bari Aldo Moro, 70125 Bari (Italy).*
[f.] *CNR, Istituto di Fotonica e Nanotecnologie, Sede di Bari, 70125 Bari (Italy).*
*Corresponding Authors: davide.blasi@uniba.it; paolo.bollella@uniba.it;

ARTICLE

Introduction

Self-assembling structures can be potentially used for many applications within the development of devices like biosensors based on different transduction techniques such as electrochemistry, quartz-crystal microbalance (QCM), surface plasmon resonance (SPR) and field-effect transistors (FETs) [1–4]. Recently, bioelectronic label-free sensors based on an electrolyte-gated organic field-effect transistor (EGOFETs) have been proposed as highly sensitive devices that involve an ionic conducting electrolyte as dielectric and connects the transducing gate electrode with an organic semiconductor-based channel[5]. Gate electrodes are usually modified with organic self-assembled structures to efficiently immobilize the biorecognition element (*e.g.,* antibodies, aptamers etc.).[6,7] By this means, trillions of biorecognition elements can be immobilized on a millimetre-sized gate enabling the single-molecule detection.[8]

Among the organic self-assembled structures, self-assembled monolayers (SAMs) of alkanethiols have been used to modify gold surfaces to achieve the formation of a densely and ordered biolayer through the immobilization of antibodies, enzymes, DNA/RNA, aptamers, whole cells etc.[9–11] In particular, SAMs of alkanethiols on gold surfaces are able to produce a stable and structurally well-defined monolayer with a controllable thickness and desirable functions on the surface (*e.g.,* different exposed functional groups like -COOH, -OH, $-NH_2$, $-OCH_3$, CH_3 *etc.*). These features were reported in several studies.[12–14] For instance, Hubbard *et al.* investigated the electrochemical behaviour and the structure of several quinone derivatives (*e.g.,* quinone moieties conjugated with alkanethiols) deposited on platinum electrodes by using several surface analysis techniques like low energy electron diffraction (LEED), Auger electron spectroscopy *etc.*[15] Moreover, the reversibility of the redox reaction analysis was used to make kinetics considerations on the reorganization of the SAM.

Indeed, SAM investigations have been performed using cyclic voltammetry and electrochemical impedance spectroscopy (EIS) to analyse the electron transfer, the ionization of the surface head group, and the ionic permeation of the layer at the interface.[16,17] Electrochemical probes (*e.g.,* $[Fe(CN)_6]^{3-/4-}$, $[Ru(NH_3)_6]^{3+/2+}$ *etc.*) are usually employed to study the defect sites and interchain reorganization in SAM surfaces induced by electrochemical desorption as well as its effect on the electron transfer process. Moreover, also optical techniques provide useful structural information. Particularly, *in situ* Fourier-transform IR reflection absorption spectroscopy (FT-IRRAS) measurements have been applied to study the structure and the orientation of SAMs.[18] Alternatively, attenuated total reflection (ATR) also provides insights on the chemical composition of the self-assembled structure and possible interchain interactions driving the reorganization process over time.[19]

This work aims at investigating the interpenetration of negatively charged electroactive ions to probe the interchain reorganization of a SAM endowed with hydrogen bonding, namely the N-(2-hydroxyethyl)-3-mercaptopropanamide (NMPA) in the presence of an external electric field. For the sake of comparison, a 1-hexanethiol SAM, bearing no hydrogen bonding, is studied as well. To this end, cyclic voltammetric measurements of an electroactive negatively charged probe - $Fe(CN)_6^{4-}$ - at a gold working electrode modified with the elicited SAMs, are performed. The SAMs coverages are heterogeneous and multiple defects or pinhole sites are present. The kinetics and the diffusional/interpenetration data of the probing species over time provides key information on the interchain reorganization in the electric field. These results can be of interest in the design of high performance bioelectronic devices, particularly EGOFETs, where the effect of ions diffusion on the building of the charge double layers as well as their permeation into SAMs modified gate electrodes, plays a key role in the understanding of the working principle.[20–22]

Materials and Methods

Materials

1-hexanethiol was purchased from Sigma-Aldrich and used without further purification. N-(2-hydroxyethyl)-3-mercaptopropanamide (NMPA) was prepared starting from 3-mercaptopropionic acid (3MPA) using a wet chemical approach described elsewhere.[23] A phosphate buffered saline (PBS, Sigma-Aldrich) (phosphate buffer of 10 mM, KCl 2.7 mM, NaCl 137 mM) tablet was dissolved in 200 mL of HPLC water and used upon filtration on a Corning 0.22 µm polyethersulfone membrane. Potassium Ferrocyanide $K_4[Fe(CN)_6]$ was purchased by Sigma Aldrich and dissolved in a PBS solution to obtain a 10 mM solution. This solution was diluted 1:10 in PBS before the Cyclic Voltammetry measurement. All solutions were prepared using Milli-Q water (18.2 MΩ cm, Millipore, Bedford, MA, USA).

Sample Preparation

Gold samples were prepared starting from a Si Wafer covered by a thermally grown 300 nm thick SiO_2 layer. The substrates were cleaned through ultrasonic bath in acetone for 10 minutes, then in isopropanol (10 min) and subsequently dried under a N_2 flux. Afterwards, e-beam evaporation of a 5 nm-thick Ti adhesion layer followed by a 50 nm-thick gold film has been performed through a shadow mask. The gold sample, shown in figure 1, comprises a 20 mm^2 circular pad, being the sample active area, connected to a 25

mm^2 square contact pad through a 500 mm-thick track. Prior to the self-assembled monolayer (SAM) growth on the gold active area, the samples were sonicated for 10 min in heptane, then rinsed with acetone and dried under N_2 flux. Afterwards, the samples were immersed in a Piranha Solution (H_2O_2:H_2SO_4 3:7 v/v) for 5 min, then in boiling water for 10 min, rinsed with ethanol and dried under N_2 flux. Finally, the samples were treated with Ozone Plasma for 10 min and immediately immersed in the 10 mM thiol SAM solution for 20 h in N_2 atmosphere and in the dark. Two different SAMs were used in this work, characterized by different interaction between chains: the NMPA presents an amide in γ position respect to the sulphur atom, so SAMs growth using this precursor presents a diffuse interchain hydrogen bonding[24,25] resulting the most intense interaction between all the samples. 1-hexanethiol is a six-carbon alkyl chain and SAMs growth using this precursor are characterized by the weakest chain interaction. Before the electrochemical characterization, the samples were rinsed with ethanol to remove possible unbounded residues and dried under N_2 flux. Before the optical characterizations, samples were rinsed with HPLC water and dried under N_2 flux.

Modelling Analysis

The equations were discretized by the finite difference method (FDM) and numerically solved using an explicit Euler scheme. The proposed model for cyclic voltammetry outputs was implemented in MATLAB® language. The positive currents in the voltammogram corresponds to the oxidation process (anodic current), whereas the negative currents represent the reduction process (cathodic current), according to IUPAC recommendation.

Cyclic Voltammetry

Cyclic voltammetry (CV) measurements were performed with a CH-1140b potentiostat-galvanostat (CH Instruments, Bee Caves, TX, USA). A conventional three electrode electrochemical cell setup was used for all the experiments, encompassing a platinum wire as counter electrode (CE), an Ag/AgCl (saturated KCl) electrode as reference electrode (RE) (notably all potential values in the manuscript are reported *vs* this reference electrode) and the gold electrode, eventually modified with the two different SAMs (*vide supra*), as working electrode (WE). A schematic viewgraph of the electrochemical cell is reported in figure 1B. All the measurement were carried out in a 1 mM $K_4[Fe(CN)_6]$ solution in PBS. The measurements were performed using a potential window ranging from -0.3 to 0.6 V at 100 mV s^{-1} scan rate. The CVs reported in the paper were extracted from the last scan (4th scan). Starting potential was set at the Open Circuit Potential value, measured at the beginning of the experiment. The sample was left in the cell for a total of 210 min and CV measurements were carried out after 0, 20, 30, 60, 90, 120, and 210 min from the beginning of the experiment. The data were treated using OriginPro 2018.

Grazing Angle – Attenuated Total Reflectance (GA-ATR)

(GA-ATR) infrared analyses were carried out by using a Perkin Elmer Spectrum Two FT-IR spectrometer equipped with an ATR module including a diamond crystal at a fixed 45° incidence angle, as shown in figure 1C. Each spectrum was mediated over 64 scans in the range 400-4000 cm^{-1}, at a spectral resolution of 2 cm^{-1}. The presence of a gold layer under the SAM permits to create a configuration equivalent to the so-called Grazing Angle – Attenuated Total Reflectance (GA-ATR).[26,27,28] In principle, considering the penetration depth of the evanescent wave (some µm), a SAM layer should be too thin (1 nm) to be detected by conventional ATR. However, the presence of the metal/SAM interface in the proximity of the ATR crystal results in an increase of the electric field in the SAM layer, enhancing the signals associated to the vibrational transitions.[28,29] Each sample was analysed in the circular area for a total of 2 points for each sample.

Results and Discussion

Evaluation of NMPA surface coverage

To assess the surface coverage of NMPA SAM onto the Au electrode surface, reiterated cyclic voltammograms (CVs) in 0.5 M H_2SO_4, were performed in the -0.2 V and +1.7 V range. The data are given in figure 2. The working electrode was either bare gold (figure 2, black line) or the NMPA SAM modified gold electrode (figure 2, red line). The gold electrode shows the well-known broad oxidation wave between +1.1 V and +1.4 V due to the formation of gold oxide. In the reverse scan the sharp cathodic peak (peak current of -95 µA) in the range of +1 V to +0.8 V is the corresponding reduction process. In addition, there is a peak at 0.0 V that can be ascribed either to the presence of active metal atoms at the electrode surface or to the electrocatalytic reduction of oxygen at gold [30] As it is apparent, a suppression of the gold reduction/oxidation occurs in the presence of the NMPA SAM.

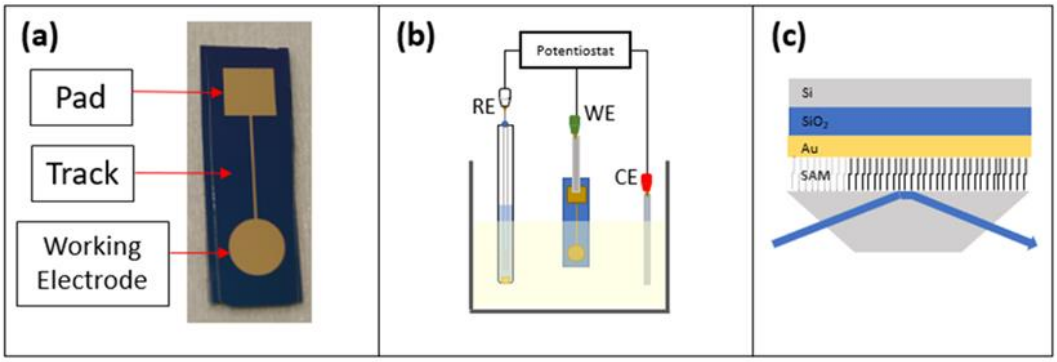

Figure 1 a) the working electrode comprises the circular area that is immersed during the experiment, whereas the square pad is the contact and a thin track connects these areas; b) the CVs is a standard three electrode cell encompassing an Ag/AgCl *reference electrode (RE), the working (WE) given in panel (a) and a platinum wire serving wire as counter (CE); c) the GA-ATR configuration for the measurements of the SAM IR spectra.*

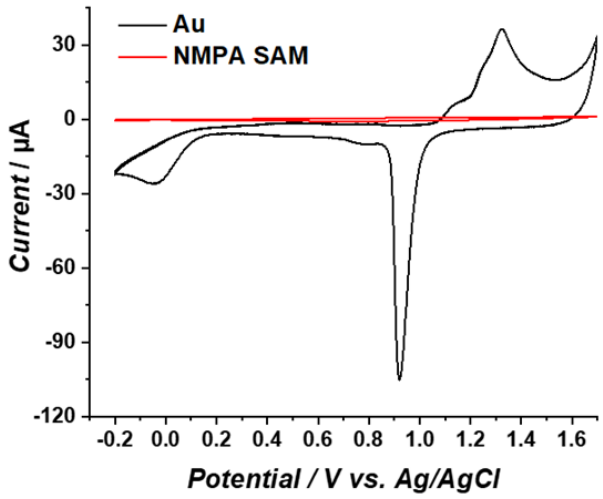

Figure 2: CVs measured for bare Au (black curve) and NMPA SAM (red curve) in 0.5 M H_2SO_4 at a scan rate of 50 mV s^{-1} and at T = 25°C

A significant decreasing in the current associated with the charging of the double layer capacitance is also seen. Indeed, similarly to an alkanethiol, NMPA can act as an impermeable material hindering water/ions access to the gold surface, hence impairing its electrochemical oxidation. The effective Au electrode surface area was estimated from the reduction peak resulting in a charge involved of 47.8 µC. This value can be normalized by the theoretical charge density considered for gold oxide reduction (390 µC cm^{-2}), as reported in the literature,[31] returning an effective active surface area of 12 mm^2. This means that only the 60% of the geometrical area (notably 20 mm^2) is electrochemically active.

Considering that this peak is totally disappearing after the formation of NMPA SAM, we can assume that this part of the electrode surface is totally covered with the NMPA SAM. Similar results were previously reported in the literature considering other types of SAMs.[32–34]

Modelling the Electroactive Ions Permeation at the SAM modified Electrode Surface

To fully comprehend how the negative ions of a redox couple can probe the SAM film, it is relevant to understand the effect of ions penetration in a SAM structure and its possible rearrangements both from theoretical and experimental point of view. In this respect, it is important to consider the equations behind the permeation/diffusion of ions during the electrochemical processes occurring at the modified electrode surface.[35] Considering $K_4[Fe(CN)_6]$ as a model compound A_1, it is possible to write the following equations:

$$A_1 \underset{k'_2}{\overset{k_1}{\rightleftharpoons}} A_2 \quad K = k_1/k_2 \quad (1)$$

$$A_2 + e^- \rightleftharpoons B_2 \quad E^{0\prime} = (E_{pa} + E_{pc})/2 \quad (2)$$

$$B_2 \rightleftharpoons B_1 \quad K' = k'_1/k'_2 \quad (3)$$

where the partition equilibria (equations 1 and 3) are occurring at the interface between the electrode surface modified with the NMPA and the solution containing the diffusing redox probe, namely $K_4[Fe(CN)_6]$. The electrochemical reaction occurring at the electrode surface (equation 2), involving the permeation/diffusion of an ionic redox probe and its subsequent electrochemical reaction needs to be described too. A best suited model involves a Chemical-Electrochemical-Chemical (CEC) process where the chemical part is for instance a partition-reaction. This process is also schematically displayed in figure 3.

Both partition equilibria, notably for the reactant A and the product B in both phases (*i*= 1, 2), can be analytically described with the Fick's law on the diffusion:

$$\frac{\partial A_i}{\partial t} = D_i \frac{\partial^2 A_i}{\partial x^2} \quad (4).$$

Thus, considering the boundary conditions at the electrode/solution interface (x=1), it is possible to obtain:

$$D_1 \frac{\partial A_1}{\partial x}\Big|_{x=1} = D_2 \frac{\partial A_2}{\partial x}\Big|_{x=1} = k_1 A_1|_{x=1} - k_2 A_2|_{x=1} \quad (5)$$

$$D_1 \frac{\partial B_1}{\partial x}\Big|_{x=1} = D_2 \frac{\partial B_2}{\partial x}\Big|_{x=1} = k'_1 B_1|_{x=1} - k'_2 B_2|_{x=1} \quad (6)$$

where $K = k_1/k_2$ and $K' = k'_1/k'_2$ are the equilibrium constant pertaining the heterogeneous reaction (equations 1 and 3).[36] On the other hand, the electrochemical reaction occurring at the electrode surface (x=0) can be analytically described by the Butler-Volmer equation as follows:

$$i = nFSk_0 \left(A_2|_{x=0} exp\left(-\frac{\alpha F\left(E-E^{0\prime}\right)}{RT}\right) - B_2|_{x=0} exp\left(\frac{(1-\alpha)F\left(E-E^{0\prime}\right)}{RT}\right)\right) =$$

$$nFSD_2 \frac{\partial A_2}{\partial x}\Big|_{x=0} = -nFSD_2 \frac{\partial B_2}{\partial x}\Big|_{x=0} \quad (7)$$

where n (number of electrons transferred in the electrochemical reaction), F (Faraday's constant and 96485 C mol^{-1}) and S (electroactive surface area) have their usual meaning.[37] The last equation describes the variation of the net current passing through a working electrode that depends on the voltage difference between the voltage required for a redox reaction to occur at the electrode surface (oxidation or reduction) and the formal potential ($E^{0\prime}$, equilibrium potential or bulk electrolyte potential), defined as overpotential. Butler-Volmer equation, as reported above, allows to make calculation on the electro-kinetics parameters still considering mass-transfer limitations related to the electrode modification but

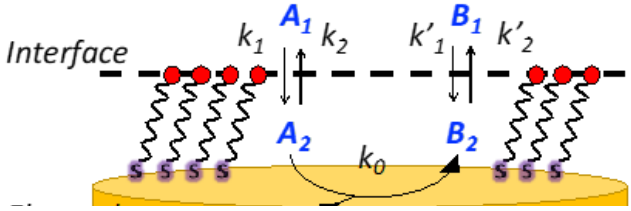

Figure 3: Schematic representation of the partitioning of reactant A and product B at the interface solution/modified electrode.

also to the electrochemical process itself. This system of equations overview on the dynamics of permeation/diffusion and electrochemical reaction occurring at a SAM modified electrode.
Hence considering the faradaic current measured on the NMPA SAM given in figure 2 (red curve), equations 5, 6 and 7, a given diffusing probe A exchanging one electron (n = 1) and an effective area S = 12 mm^2, the heterogeneous electron transfer rate constant (k_{ET}) is (0.45 $\pm$ 0.05) 10^{-3} cm s^{-1}cm s^{-1}. This is compatible with a k_{ET} obtained in the presence of a blocking interface (hindering ions penetration and interchain rearrangements) based on SAMs modified electrodes[38].

Probing a Au-SAMs electrode with a redox active negative ion

To probe the ion permeation/diffusion in a SAM, a cyclic voltammetry experiment is designed involving a Au working electrode modified with SAMs encompassing different functional groups, namely the already introduced NMPA and the 1-hexanethiol SAM. The main difference is the interchain hydrogen bonding that is present only in the NMPA SAM. The probe is the $[Fe(CN)_6]^{4-}$ negatively charged redox probe, discharging (exchanging electrons) at the Au-SAM working electrode. Reiterated cyclic voltammetry curves are measured to assess how the current and voltage peak positions shift over time or equivalently under the application of an external electrical field. As already demonstrated, the electric field between the working and the counter electrodes induces a reorganization of the SAM's chains that can be tighten up and create a barrier hindering to a given extent, the diffusion of ions at the electrode surface.[39] This is even more true in the presence of amide functional groups that originates an hydrogen bond with its associated dipole moment oriented from the oxygen of the amide group in one chain and points towards the hydrogen of the amide group of a neighbouring one. Because of the regular assembly of the NMPA-SAM, an H-bonding network likely forms that, thanks to the elicited dipole, better orients in an electric field.
The electron transfer (ET) at a SAM modified electrode can occur, following one of three pathways: (1) by a tunnelling process; (2) by permeation of the redox species into the film and ET; and (3) by diffusion of the redox probe inside pinholes or defect sites and ET only at the exposed electrode surface.[40,41] Case (1) requires the SAM to be totally homogeneous and defect free, case (2) requires the film to be ion-permeable, while case (3) occurs when the SAM has pinholes or defect sites. To assess the SAM homogeneity and degree of defects, the CVs kinetics is studied by acquiring the CV curve at different times (0, 20, 30, 60, 90, 120, and 210 minutes) on the NMPA and 1-hexanethiol SAM as well as on bare gold. Longer times means longer exposure to an external electric field. The measured CV curves are displayed in figures 4 A-B-C, respectively. The CVs over time for the NMPA modified gold electrode (notably from 0 to 210 minutes; recorded at 0, 20, 30, 60, 90, 120 and 210 minutes, figure 4 A) exhibit a clear peak potential shift and a slight current decrease. The cathodic peak is progressively moving towards negative values, while the anodic peak is gradually moving in the opposite direction.
The NMPA SAM, encompassing alkyl chains with -NH groups at half height and -OH groups exposed towards the solution interface, are densely packed and well-organized acting as an effective electron and ion barrier. In the presence of this monolayer, $[Fe(CN)_6]^{4-}$ cannot directly approach the electrode surface thus decreasing its apparent heterogeneous electron transfer rate. This effect is

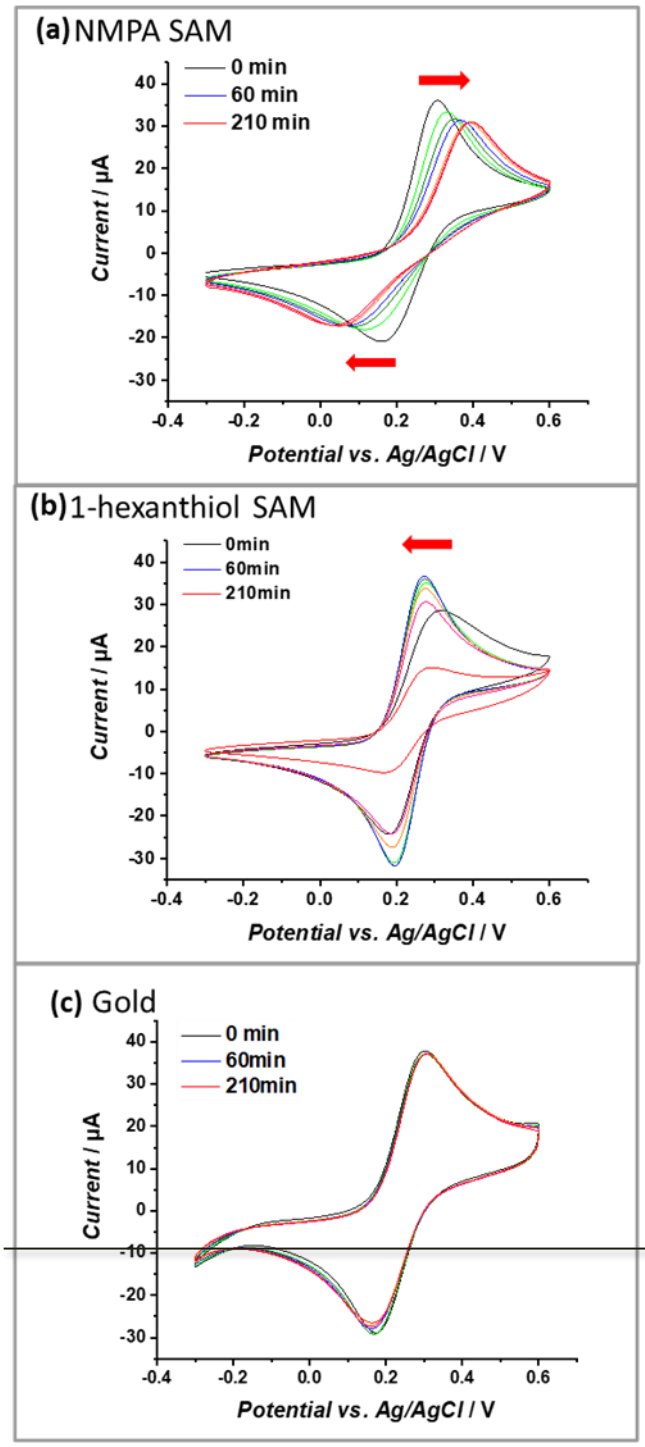

Figure 4: CVs measured for a) NMPA SAM, b) 1-hexanethiol SAM and c) bare Au in 1 mM $K_4[Fe(CN)_6]$. Experimental conditions: 10 mM PBS buffer pH 7 containing KCl 2.7 mM and NaCl 137 mM; scan rate 100 mV s^{-1} and T = 25 °C. Each panel reports curves acquired on the same sample monitoring the cyclic voltammograms for a total time 210 min. The red arrows are pointing in the direction of the peak shift.

related to the elicited inter-chain hydrogen bonding between the amide groups positioned at half height of the chain,[24,25,42–45] while terminal -OH groups are mainly involved in randomly-oriented interactions with water molecules. The 1-hexanethiol SAM, forms a hydrophobic layer that however does not tighten in the external electric field. This SAM was taken into account because of its length that is comparable with NMPA but with no

amide functionalities. Here the CVs, reported in figure 4 B, showed a perfectly reversible or quasi-reversible behaviour over time as the potential difference between the anodic and cathodic peak is not varying. This might be in contradiction with other reports where 1-hexanethiol SAM exhibited an irreversible behaviour.[46] However, the heterogeneous formation of 1-hexanethiol SAM as well as the random reorganization mainly affected by the hydrophobic forces might have created some pinholes or defect sites that allowed ferrocyanide ions to diffuse directly at the electrode surface. Besides the kinetic considerations on the ET, it is possible to observe that the faradaic current peaks for both processes (anodic/oxidation and cathodic/reduction) are dropping quite significantly over time meaning that the permeation of $[Fe(CN)_6]^{4-}$ is hindered by the hydrophobic layer, which is in agreement with other reports. Hence, the kinetics of the ET process occurring at the pinholes is predominantly affecting the electrode behaviour while from the ion permeation/diffusion perspective the hydrophobic layer is showing the predominant effect.

This has been further confirmed by the CVs over time for the bare gold electrode. Figure 4 C showed no peak shift both in terms of potential and current values. This effect is certainly ascribed to the absence of electrostatic interactions (no functional groups are present) with the redox probe.

These results can be further analyzed by plotting the faradaic current of the anodic process over time (cathodic process showed exactly the same trend but with current values in the negative range), as displayed in figure 5. Bare gold electrode (black squares) showed no variations over time because there is only the electrochemical process taking place at the electrode with no diffusing barriers. NMPA SAM modified electrode reached a steady-state level after 50 minutes, corresponding to an effective reorganization (mainly due to the presence of amide groups that are driving the reorganization in the electric filed) and the exposed uncharged -OH groups that are not hindering the interpenetration of negatively charged ions. Moreover, we have compared the results with 1-hexanethiol modified electrode where the pinholes/SAM defects are predominantly affecting the faradaic current at the beginning of the experiment. Approximately 30-60 minutes later, the SAM chains rearrangement driven by the alkyl-chains lipophilic interactions tighten the film structure and the faradaic current is remarkably decreasing due to the diffusion barrier generated by the interchain rearrangement. To validate our hypothesis, we fitted the experimental data (current *vs* time) using a combination between the equation 7 (derived from Butler-Volmer equation) and the equation 8 (notably, Nicholson and Shain equation). The equation was further rearranged considering that the electron transfer can slow down due to a diffusional barrier formed by the SAM chains undergoing reorganization process. All data sets, notably NMPA modified electrode (figure 5, red curve), 1-hexanethiol modified electrode (figure 5, blue curve) and bare gold electrode (black curve), were fitted returning a regression factor R^2= 0.99.

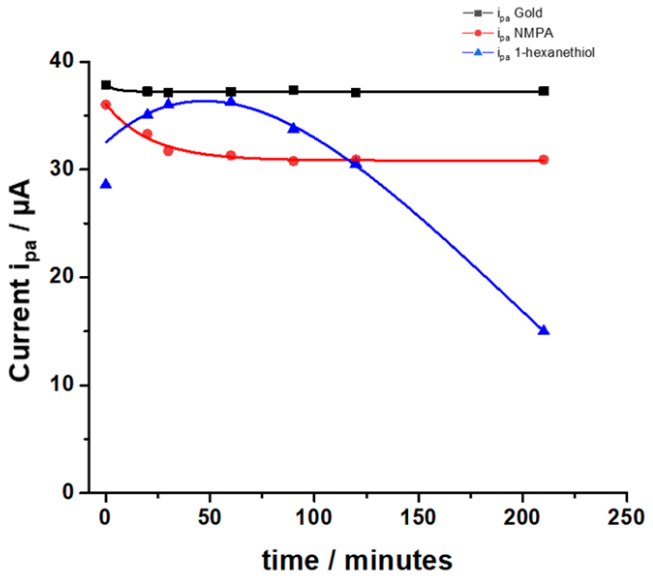

Figure 5: Anodic peak currents measured for NMPA SAM (red line), 1-hexanethiol SAM (blue line) and bare Au (black line) in 1 mM $K_4[Fe(CN)_6]$. Experimental conditions: 10 mM PBS buffer pH 7 containing KCl 2.7 mM and NaCl 137 mM; scan rate 100 mV s^{-1} and T = 25°C. The fitting of the experimental points was performed combining the equations 7 and 8, where the electron transfer rate constant (k_0) was computed considering the electron transfer reaction occurring at the modified electrodes.

The diffusional data are further supported by the calculation of the heterogeneous electron transfer rate constant (k_0) performed at the time 0 and after 210 minutes. k_0 was calculated using the extended method which merges the Kliengler-Kochi and Nicholson-Shain methods for totally irreversible and reversible systems, respectively.[47,48] For a one-step *quasi*-reversible electrochemical reaction in which the kinetic parameter $\Psi=k^0[\pi DnvF/(RT)]^{-1/2}$ is varying up to 0.1 and the ΔEp x n not exceeding 200 mV, the Nicholson and Shain method should be valid considering the working curve Ψ-$\Delta Ep\ x\ n$ followed by a Ψ-$v^{-1/2}$ plot. [49] On the other hand, Kliengler and Kochi method allows the calculation of ET rate constant k_0 for irreversible system by following the equation below reported:

$$k_0 = 2.18\left[\frac{D\beta nvF}{RT}\right]^{\frac{1}{2}} e^{-(\frac{\beta^2 nF}{RT})(E_p^a - E_p^c)} \qquad (8)$$

where β is the ET coefficient for the redox process considered and E_p^a-E_p^c the peak-to-peak separation between the anodic and the cathodic peak, which should be higher than 200 mV out of Nicholson and Shain method. Herein, the evaluation of the ET rate constant k^0 was performed by using an extended method reported in the literature, considering every redox system (quasi-reversible and irreversible) over the whole peak separation interval. The equation 8 was rearranged as follow:

$$\Psi = 2.18\left[\frac{\beta}{\pi}\right]^{\frac{1}{2}} e^{-\frac{\beta^2 F}{RT} n\Delta E_p} \qquad (9)$$

where the symbols have their usual meaning. Finally, the k_0 could be easily calculated from the slope of the graph Ψ-$[\pi DnF/(RT)]^{-1/2}\ v^{-1/2}$. At t=0, k_0 resulted to be (0.3 ± 0.05) 10^{-3}

cm s^{-1}, which decreased remarkably by almost two orders of magnitude as (0.4 ± 0.05) 10^{-5} cm s^{-1}. These results are in agreement with the theoretical model applied in the previous model and with the diffusional data analysed in this section, hence confirming the interchain NMPA SAM reorganization due to the intercalation of negatively charged ions.

Grazing-Angle ATR Investigation of NMPA SAM Reorganization on a Gold Electrode

GA-ATR is a very useful tool to study SAMs grafted on very high refractive index metal, thanks to the enhance of the signal described in the Methods section. Moreover, the metal-surface selection rule in IR techniques, where only the component perpendicular to the surface is active,[24,50] can be useful in gathering structural information on amide-based SAMs. In fact, the dipole moment of amides groups main IR signals, namely the C=O stretching (amide I) and the N-H bending (amide II), are oriented perpendicular to each other. Hence, the ratio between these signals can be used to evaluate the chain orientation with respect to the metal surface.[24] To investigate the effect of the reiterated CVs in the $Fe(CN)_6]^{4-}$, with its associated bias applied perpendicular to the metal surface, an NMPA SAM on Au was analysed by GA-ATR IR spectroscopy before (figure 6a) and after a CV experiment (figure 6b).

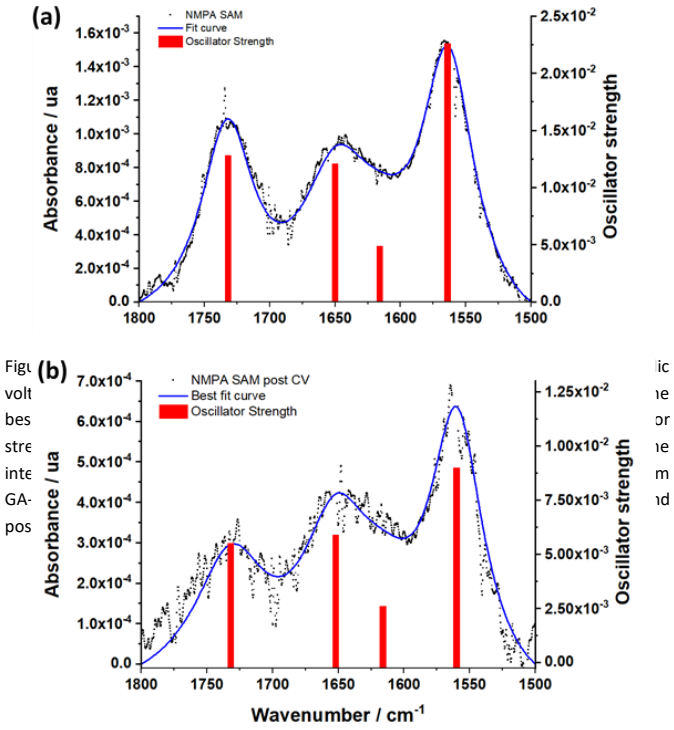

Fig volt bes stre inte GA- pos ic ıe or ıe m ıd

Both spectra present two main peaks associated to the Amide I (1650 ± 1 cm^{-1}) and the Amide II (1570 ± 1 cm^{-1}) signals. *A peak centred at 1731 ± 1 cm^{-1} is attributed to traces of fatty acids on the substrate, residues of the cleaning procedure and found in previous works*[51]*. Moreover, the presence of a fourth peak around 1630-1600 cm^{-1} was hypothesized, resulting a shoulder in the amide I peak. The experimental curves are accurately reproduced by a model based on light-matter interaction with a multi-layer structure, including 4 harmonic oscillators. The presence of a harmonic oscillator at 1615 cm^{-1} confirmed the presence of the fourth peak hypothesized above."* To evaluate the changes after the cycling in $K_4[Fe(CN)_6]$, we used the ratio between the oscillators strengths associated to the Amide I and Amide II bands, as extracted by the fitting procedure. The Amide I/Amide II ratio in the spectrum in fig. 6a is equal to 0.53, whereas in the spectrum 6b the value increases to 0.66 (19%), evidencing a clear reorientation of the NMPA chains when an external electric field is applied. In particular, the N-H dipole moment z-component (perpendicular to the gold surface) becomes lower while the C=O z-component increases (figure 7).

Hence, the GA-ATR data are clearly proving that the amide groups present at half-chain are playing a key role in the interchain NMPA SAM reorganization; specifically, after the application of an external field the chains are bent forming a larger angle with the normal to the surface. Actually, Kim et *al.* reported two different phases, characterized by different tilt angles, for an amide-containing alkanethiol SAM deposited on gold {111} from ethanolic solution. In particular, while at room temperature the two phases coexist, increasing the temperature during the SAM formation, or performing a thermal annealing, the system assumes the more tilted configuration [45], that is thermodynamically favoured due to the formation of linear hydrogen-bonding networks[52]. Hence, the application of an external electrical field can act as the temperature in forcing the SAM in its more stable configuration.

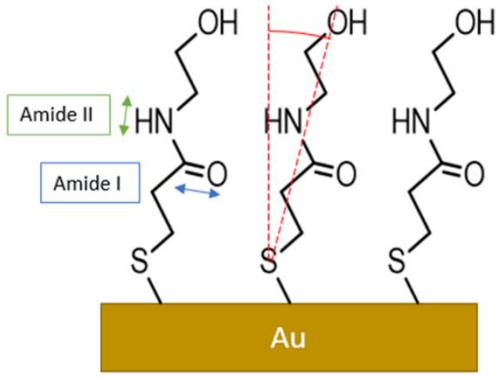

Figure 7: NMPA SAM on Au gate structure. Direction for dipole moments associated to the amide I and amide II signals are reported as blue and green double arrow, respectively. Red arc indicates the ϑ angle between surface normal and chain direction. The sketch is not in scale and exaggerated to make the orientation more evident.

Conclusions

In conclusion, the characterization of two SAMs, namely NMPA and 1-hexanethiol, has been performed by using a combined method based on cyclic voltammetry (CV) and grazing angle–attenuated total reflectance (GA-ATR). NMPA SAM showed a heterogeneous surface coverage of the electroactive surface area considering the presence of SAM defects and pinholes. Upon electric field application over time, NMPA SAM chains exhibited peculiar rearrangement on the electrode surface responsible for the remarkable decreasing of the electron

transfer rate constant (k^0) by two orders of magnitude from (0.3 $\pm$ 0.05) $\cdot 10^{-3}$ cm s^{-1} to (0.4 $\pm$ 0.05) $\cdot 10^{-5}$ cm s^{-1}. Moreover, this is in agreement with ions diffusion/permeation that achieves a steady-state condition in approximately 30 minutes, when the applied electric field affects mainly contributes to NMPA interchain rearrangements. This has been further elucidated with GA-ATR IR data that are unequivocally proving NMPA SAM chains bending forming a larger angle with the normal to the surface, upon electric field application. Conversely, 1-hexanethiol SAM rearrangement was not affected by the applied electric field showing a remarkable decrease of the anodic peak current (i_{pa}) due to random reorientation of aliphatic chains that are hindering ions diffusion/permeation.
This combined investigation method can open different avenues to understand the rearrangement of SAM chains upon the application of an electric field, which is important in the design of high performance bioelectronic devices.

Author Contributions

A.T. performed the experimental work and analysed the data. A.S. and F.L. synthesized NMPA. R.A.P. supervised A.T. during the electrochemical experiments. E.M. supervised A.T. during substrate preparation (gold deposition and SAM preparation). A.F. and G.S. performed the optical measurements, analysed the data and contributed to the present draft. D.B. conceived part of the experimental work, analysed the data and contributed to the present draft. P.B. and L.T. actively wrote the manuscript draft. All the authors have read and approved the final version.

Conflicts of interest

The authors declare no conflict of interest.

Acknowledgements

PON SISTEMA (MIUR), H2020 - Electronic Smart Systems – SiMBiT: Single molecule bio-electronic smart system array for clinical testing (Grant agreement ID: 824946), ‘‘PMGB -Sviluppo di piattaforme meccatroniche, genomiche e bioinformatiche per l’oncologia di precisione’’ – ARS01_01195 – PON ‘‘RICERCA E INNOVAZIONE’’ 2014–2020 projects, Academy of Finland projects #316881, #316883 ‘‘Spatiotemporal control of Cell Functions’’, #332106 “ProSiT - Protein Detection at the Single-Molecule Limit with a Self-powered Organic Transistor for HIV early diagnosis”, Biosensori analitici usa-e getta a base di transistori organici auto-alimentati per la rivelazione di biomarcatori proteomici alla singola molecola per la diagnostica decentrata dell’HIV (6CDD3786) Research for Innovation REFIN - Regione Puglia POR PUGLIA FESR-FSE 2014 / 2020, the European Union, Italian Government, Åbo Akademi University CoE “Bioelectronic activation of cell functions” and CSGI are acknowledged for partial financial support.

Notes and references

1 A. L. Eckermann, D. J. Feld, J. A. Shaw and T. J. Meade, *Coord. Chem. Rev.*, 2010, **254**, 1769–1802.

2 M. Tominaga, A. Ohira, Y. Yamaguchi and M. Kunitake, *J. Electroanal. Chem.*, 2004, **566**, 323–329.

3 K. V. Gobi, K. Matsumoto, K. Toko, H. Ikezaki and N. Miura, *Anal. Bioanal. Chem.*, 2007, **387**, 2727–2735.

4 S. Casalini, C. A. Bortolotti, F. Leonardi and F. Biscarini, *Chem. Soc. Rev.*, 2017, **46**, 40–71.

5 D. Blasi, F. Viola, F. Modena, A. Luukkonen, E. MacChia, R. A. Picca, Z. Gounani, A. Tewari, R. Österbacka, M. Caironi, Z. M. Kovacs Vajna, G. Scamarcio, F. Torricelli and L. Torsi, *J. Mater. Chem. C*, 2020, **8**, 15312–15321.

6 F. Leonardi, A. Tamayo, S. Casalini and M. Mas-Torrent, *RSC Adv.*, 2018, **8**, 27509–27515.

7 L. Macchia, E., Manoli, K., Holtzer, B., Di Franco, C., Torricelli, F., Picca, R. A., ... & Torsi, in *2019 IEEE 8th International Workshop on Advances in Sensors and Interfaces (IWASI)*, 2019, pp. 221–223.

8 E. Macchia, K. Manoli, B. Holzer, C. Di Franco, M. Ghittorelli, F. Torricelli, D. Alberga, G. F. Mangiatordi, G. Palazzo, G. Scamarcio and L. Torsi, *Nat. Commun.*, , DOI:10.1038/s41467-018-05235-z.

9 E. Macchia, A. Tiwari, K. Manoli, B. Holzer, N. Ditaranto, R. A. Picca, N. Cioffi, C. Di Franco, G. Scamarcio, G. Palazzo and L. Torsi, *Chem. Mater.*, 2019, **31**, 6476–6483.

10 P. Bollella, F. Mazzei, G. Favero, G. Fusco, R. Ludwig, L. Gorton and R. Antiochia, *Biosens. Bioelectron.*, 2017, **88**, 196–203.

11 E. Macchia, K. Manoli, C. Di Franco, R. A. Picca, R. Österbacka, G. Palazzo, F. Torricelli, G. Scamarcio and L. Torsi, *ACS Sensors*, 2020, **5**, 1822–1830.

12 C. D. Bain and G. M. Whitesides, *Adv. Mater.*, 1989, **1**, 110–116.

13 T. Hamann, L. Kankate, E. Böhler, J. H. Bredehöft, F. M. Zhang, A. Gölzhäuser and P. Swiderek, *Langmuir*, 2012, **28**, 367–376.

14 Y. Arima and H. Iwata, *J. Mater. Chem.*, 2007, **17**, 4079–4087.

15 J. Y. Gui, D. A. Stern, D. G. Frank, F. Lu, D. C. Zapien and A. T. Hubbard, *Langmuir*, 1991, **7**, 955–963.

16 R. Schweiss, C. Werner and W. Knoll, *J. Electroanal. Chem.*, 2003, **540**, 145–151.

17 K. Kim and J. Kwak, *J. Electroanal. Chem.*, 2001, **512**, 83–91.

18 S. Ye, A. Yashiro, Y. Sato and K. Uosaki, *J. Chem. Soc. - Faraday Trans.*, 1996, **92**, 3813–3821.

19 M. Bieri and T. Bürgi, *J. Phys. Chem. B*, 2005, **109**, 10243–10250.

20 E. Macchia, K. Manoli, C. Di Franco, G. Scamarcio and L. Torsi, *Anal. Bioanal. Chem.*, 2020, **412**, 5005–5014.

21 R. A. Picca, K. Manoli, E. Macchia, L. Sarcina, C. Di Franco, N. Cioffi, D. Blasi, R. Österbacka, F. Torricelli, G. Scamarcio and L. Torsi, *Adv. Funct. Mater.*, 2020, **30**, 1904513.

22 E. Macchia, K. Manoli, B. Holzer, C. Di Franco, R. A. Picca, N. Cioffi, G. Scamarcio, G. Palazzo and L. Torsi, *Anal. Bioanal.*

Chem., 2019, **411**, 4899–4908.

23 D. Blasi, L. Sarcina, A. Tricase, A. Stefanachi, F. Leonetti, D. Alberga, G. F. Mangiatordi, K. Manoli, G. Scamarcio, R. A. Picca and L. Torsi, *ACS Omega*, 2020, **5**, 16762–16771.

24 R. S. Clegg and J. E. Hutchison, *Langmuir*, , DOI:10.1021/la960825f.

25 O. M. Cabarcos, A. Shaporenko, T. Weidner, S. Uppili, L. S. Dake, M. Zharnikov and D. L. Allara, *J. Phys. Chem. C*, 2008, **112**, 10842–10854.

26 D. and Allara and J. Stapleton, *Surface science techniques*, 2013, vol. 51.

27 S. A. Swanson, R. McClain, K. S. Lovejoy, N. B. Alamdari, J. S. Hamilton and J. C. Scott, *Langmuir*, 2005, **21**, 5034–5039.

28 S. Prati, M. Milosevic, G. Sciutto, I. Bonacini, S. G. Kazarian and R. Mazzeo, *Anal. Chim. Acta*, 2016, **941**, 67–79.

29 T. Lummerstorfer, J. Kattner and H. Hoffmann, *Anal. Bioanal. Chem.*, 2007, **388**, 55–64.

30 R. F. Carvalhal, R. S. Freire and L. T. Kubota, *Electroanalysis*, 2005, **17**, 1251–1259.

31 S. Trasatti and O. A. Petrii, *Pure Appl. Chem.*, 1991, **63**, 711–734.

32 H. Shen, J. E. Mark, C. J. Seliskar, H. B. Mark Jr. and W. R. Heineman, *J. Solid State Electrochem.*, 1997, **1**, 148–154.

33 S. Campuzano, M. Pedrero, C. Montemayor, E. Fatas and J. Pingarrón, *J. Electroanal. Chem.*, 2006, **586**, 112–121.

34 J. Wang, B. Zeng, C. Fang and X. Zhou, *J. Electroanal. Chem.*, 2000, **484**, 88–92.

35 C. Cannes, F. Kanoufi and A. J. Bard, *Langmuir*, 2002, **18**, 8134–8141.

36 K. Oldham, *Adv. Eng. Softw.*, 2010, **41**, 9–12.

37 M. Ganser, F. Hildebrand, M. Klinsmann, M. Hanauer, M. Kamlah and R. McMeeking, *J. Electrochem. Soc.*, 2019, **166**, H167–H176.

38 H. Hagenström, M. J. Esplandiú and D. M. Kolb, *Langmuir*, 2001, **17**, 839–848.

39 Tabanlıgil Calam T. and E. HASDEMİR, *Comptes rendus l'Académie Bulg. des Sci.*

40 M. D. Porter, T. B. Bright, D. L. Allara and C. E. D. Chidsey, *J. Am. Chem. Soc.*, 1987, **109**, 3559–3568.

41 Y. F. Xing, S. J. O'Shea and S. F. Y. Li, *J. Electroanal. Chem.*, 2003, **542**, 7–11.

42 T. J. Lenk, V. M. Hallmark, C. L. Hoffmann, J. F. Rabolt, D. G. Castner, C. Erdelen and H. Ringsdorf, *Langmuir*, 1994, **10**, 4610–4617.

43 P. A. Lewis, R. K. Smith, K. F. Kelly, L. A. Bumm, S. M. Reed, R. S. Clegg, J. D. Gunderson, J. E. Hutchison and P. S. Weiss, *J. Phys. Chem. B*, 2001, **105**, 10630–10636.

44 H. O. Finklea, D. A. Snider and J. Fedyk, *Langmuir*, 1990, **6**, 371–376.

45 M. Kim, J. N. Hohman, A. C. Serino and P. S. Weiss, *J. Phys. Chem. C*, 2010, **114**, 19744–19751.

46 L. P. Méndez De Leo, E. de la Llave, D. Scherlis and F. J. Williams, *J. Chem. Phys.*, 2013, **138**, 114707.

47 A. Eswari and L. Rajendran, *Russ. J. Electrochem.*, 2011, **47**, 181–190.

48 R. J. Klingler and J. K. Kochi, *J. Am. Chem. Soc.*, 1980, **102**, 4790–4798.

49 I. Lavagnini, R. Antiochia and F. Magno, *Electroanal. - ELECTROANAL*, 2004, **16**, 505–506.

50 R. S. Clegg and J. E. Hutchison, *J. Am. Chem. Soc.*, 1999, **121**, 5319–5327.

51 A. Tricase, D. Blasi, A. Favia, A. Stefanachi, F. Leonetti, G. Colafemmina, L. Torsi and G. Scamarcio, *Appl. Surf. Sci.*, 2021, 149883.

52 S.-W. Tam-Chang, H. A. Biebuyck, G. M. Whitesides, N. Jeon and R. G. Nuzzo, *Langmuir*, 1996, **11**, 4371–4382.